Ann. Geophys., 26, 13–27, 2008
www.ann-geophys.net/26/13/2008/

Annales Geophysicae

Parameterisation of the chemical effect of sprites in the middle atmosphere

C.-F. Enell[1], E. Arnone[2,*], T. Adachi[3,], O. Chanrion[4], P. T. Verronen[5], A. Seppälä[5], T. Neubert[4], T. Ulich[1], E. Turunen[1], Y. Takahashi[3], and R.-R. Hsu[6]**

[1]Sodankylä Geophysical Observatory, University of Oulu, Sodankylä, Finland
[2]Dept. of Physics and Astronomy, Leicester University, UK
[3]Dept. of Geophysics, Tohoku University, Sendai, Japan
[4]Danish National Space Center, Technical University of Denmark, Copenhagen, Denmark
[5]Earth Observation unit, Finnish Meteorological Institute, Helsinki, Finland
[6]Dept. of Physics, National Cheng Kung University, Tainan, Taiwan
[*]now at: Dept. of Physical Chemistry, University of Bologna, Italy
[**]now at: Research Institute for Sustainable Humanosphere, Kyoto University, Uji, Japan

Received: 24 July 2007 – Revised: 8 December 2007 – Accepted: 17 December 2007 – Published: 4 February 2008

Abstract. Transient luminous events, such as red sprites, occur in the middle atmosphere in the electric field above thunderstorms. We here address the question whether these processes may be a significant source of odd nitrogen and affect ozone or other important trace species. A well-established coupled ion-neutral chemical model has been extended for this purpose and applied together with estimated rates of ionisation, excitation and dissociation based on spectroscopic ratios from ISUAL on FORMOSAT-2. This approach is used to estimate the NO_x and ozone changes for two type cases.

The NO_x enhancements are at most one order of magnitude in the streamers, which means a production of at most 10 mol per event, or (given a global rate of occurrence of three events per minute) some 150–1500 kg per day. The present study therefore indicates that sprites are insignificant as a global source of NO_x. Local effects on ozone are also negligible, but the local enhancement of NO_x may be significant, up to 5 times the minimum background at 70 km in extraordinary cases.

Keywords. Atmospheric composition and structure (Middle atmosphere – composition and chemistry) – Meteorology and atmospheric dynamics (Atmospheric electricity; Lightning)

1 Introduction

Electrical discharges during thunderstorms occur not only in the troposphere. In recent years a number of middle-atmospheric so-called transient luminous events (TLEs) have been discovered – best known are the red sprites (Franz et al., 1990; Sentman et al., 1995). Figure 1 shows schematically the different TLEs known. An overview of the different classes of TLE and their properties can be found in Neubert (2003) and references therein.

Electric discharges are known to have chemical effects, among the most important of which is the production of odd nitrogen (NO_x=N+NO+NO_2) and possibly odd oxygen (ozone and atomic oxygen). NO_x is long-lived in the middle atmosphere, with diurnal conversion between NO_2 at night and NO at day taking place due to photochemistry. NO_x affects the ozone profile and therefore the temperature profile of the atmosphere, coupling chemistry to dynamics. For further reading on NO_x sources and transport, we refer the reader to studies such as Callis et al. (2002) and Funke et al. (2005).

Tropospheric lightning has been shown to produce NO_x, e.g. by Noxon (1976). Many estimates of its role in the global NO_x budget have been published since then. Although available estimates differ by up to an order of magnitude, the lightning source amounts to about 10% of total tropospheric NO_x production, less than burning of fossil fuels and biomass, but comparable to soil emission. See the book by Rakov and Uman (2003) or the review by Schumann and Huntrieser (2007) for recent updated lists of estimates.

Recent observations also suggest that local production of NO_x may take place even in the upper troposphere above thunderstorms (Baehr et al., 2003). This might be associated with blue jets (Mishin, 1997), although for such cases air intrusions from the troposphere in convective systems can occur. See for example the TROCCINOX measurements

Correspondence to: C.-F. Enell
(carl-fredrik.enell@sgo.fi)

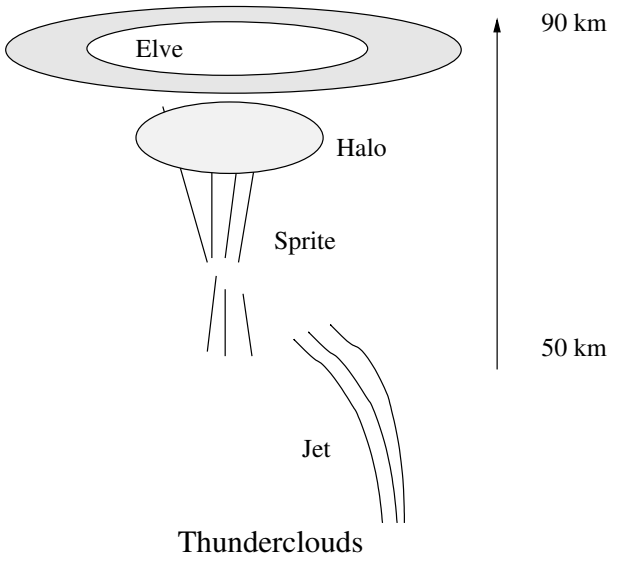

Fig. 1. Schematic overview of the different types of TLEs known.

(Huntrieser et al., 2007). Gigantic jets extending from the clouds to the ionosphere (Su et al., 2003) are long-lived and can thus potentially produce more NO_x per event than the other TLE types, but jet observations are to date very rare. Whether this is due to the low frequency of the events or the difficulty of observing blue emissions in the presence of clouds is an open question.

The energy dissipated in elves (Fukunishi et al., 1996; Mende et al., 2005) is also certainly of major interest since the very high luminosity indicates significant excitation and ionisation, although short-lived. This would be an important topic of further studies. The somewhat similar sprite halos have been considered as a source of excited atomic oxygen by Hiraki et al. (2004).

In the following, however, we concentrate on the well studied streamer discharge type of TLE, the red sprites. Auroral research pioneer Kristian Birkeland (Birkeland, 1908) is famous also for his development of a method to fixate atmospheric nitrogen through discharges. Although the temporal and spatial scales are very different, the similarity between sprites and the processes occurring in the aurora, namely excitation, ionisation and dissociation of atmospheric components by electron impact, suggests the use of a chemistry model developed for auroral conditions also in the study of sprites. The first part of this paper is a description of this use. The production of odd nitrogen and oxygen during TLE discharges is estimated for a few type scenarios. The second part of this paper discusses the significance of the results.

2 Modelling

2.1 The SIC model

Spectroscopic observations of sprites (see e.g. Mende et al., 1995; Morrill et al., 1998; Bucsela et al., 2003; Liu et al., 2006) allow estimating the rates of ionisation, dissociation and excitation of the atmospheric major species, molecular nitrogen and oxygen. To quantify the chemical effects of these processes we apply an extended version of the Sodankylä coupled Ion-neutral Chemistry (SIC) model. SIC was originally a steady-state model of ion-ion reactions (Turunen et al., 1996), but has later been developed into a 1-dimensional, fully time-dependent model suitable for case studies of the ionospheric and neutral-atmospheric chemical effects of transient forcing, such as auroral electron precipitation and solar proton events (Verronen et al., 2005; Verronen, 2006). In the current stable version (SIC 6.9.0), 36 positive ions, 29 negative ions and 15 neutral components are modelled. 17 other neutral background species are fixed, given by the MSISE-90 empirical atmospheric model (Hedin, 1991) and tables in Shimazaki (1984). Additionally the mixing ratio of water vapour is fixed to 5 ppmv below 80 km and CO_2 is fixed to 335 ppmv.

For the present work, where excitation, ionisation and dissociation of the molecular major constituents during TLEs are calculated by external models, an extended version, presently numbered SIC 7.3.9, has been developed. SIC 7.3.9 contains 17 additional excited neutral species. The additions and extensions from the standard SIC 6.9 model are summarised in Appendix A, whereas the basic principles of SIC are briefly repeated in the following.

2.1.1 Basic principles of the SIC model

The philosophy of SIC is to use a set of chemical reactions as comprehensive as possible, while keeping the mathematical algorithms simple. Since the timescales of the most important reactions span from practically instantaneous to many hours, the set of differential equations will be stiff. A suitable numerical method for such equations is the semi-implicit Euler method (Press et al., 1992), which is adopted in SIC to integrate the concentrations $\boldsymbol{N}_t$ in time over time steps τ:

$$\boldsymbol{N}_{t+\tau} = \boldsymbol{N}_t + \tau \boldsymbol{F}(\boldsymbol{N}_t)\left[\mathbf{1} - \tau \frac{\partial \boldsymbol{F}}{\partial \boldsymbol{N}}\bigg|_{\boldsymbol{N}_t}\right]^{-1} \quad (1)$$

The vector $\boldsymbol{F}(\boldsymbol{N}_t)$ is the sum of productions and losses due to all processes: excitation, ionisation, dissociation and chemical reactions. The partial derivatives of $\boldsymbol{F}$ with respect to the concentrations of the modelled species, $\partial \boldsymbol{F}/\partial \boldsymbol{N}$, are estimated by adding together the corresponding reaction rate coefficients.

In SIC, the time steps τ of Eq. (1) are exponentially increasing, i.e.:

$$\tau = T a^{N-n}, n = 1, 2, \ldots, N \quad (2)$$

where T is the main interval of integration. In normal SIC runs T is usually set to 5 or 15 min and N to 5 or 20. The constant $a<1$ is selected in order for the shortest time steps τ to be shorter than the timescale of the fastest reactions. To enable inclusion of sprite data, SIC 7.3 has been adapted to allow arbitrary unequal time intervals T down to microseconds. After each standard time interval, i.e. normally after $T=5$ or $T=15$ min, but not after shorter bursts, the photoionisation and -dissociation rates are updated, calculated following Brasseur and Solomon (2005) with solar spectra from the Solar2000 spectral irradiance model (Tobiska et al., 2000). The vertical transport of long-lived non-excited species is also calculated, using code adapted from Chabrillat et al. (2002) and Banks and Kockarts (1973).

2.1.2 Sprite modelling with SIC

The reaction rate coefficients used in SIC are allowed to be either constant or empirical functions of electron temperature T_e, neutral temperature T and pressure P, but reaction energetics are not treated explicitly. Below ≈120 km where local thermodynamic equilibrium (LTE) prevails, this approach is almost always justifiable. In discharges, however, the LTE assumption does not strictly hold true. Studies of tropospheric lightning (Balakrishnan and Dalgarno, 2003) suggest a significant production of NO_x through energetic neutral oxygen atoms (ENO) in directly NO-producing reactions such as

$$O^+ + e^* \rightarrow O^* \quad \text{(R1)}$$

$$O^* + N_2 \rightarrow NO + N \quad \text{(R2)}$$

where O^* is an ENO. Modelling such reactions is beyond the scope of the SIC model. This process is most important during the continuing return current phase of a lightning discharge, not in a propagating streamer (Coppens et al., 1998). High time resolution imaging such as by Cummer et al. (2006) and Stenbaek-Nielsen et al. (2007) show the propagating streamers to be short-lived (an emitting region of ≈25 m scale size moving at $\approx 10^7$ m/s). Hence, until observations or microphysical models confirm that significant ENO conversion takes place in sprites, we will regard the sprite streamers as a "cold" thermal plasma, for which the SIC approach is valid. The discharge tube experiments presented and discussed by Peterson et al. (2005) as well as the review by Pasko (2007) support this assumption. The production of NO_x in sprites can therefore be assumed to be initiated by

1. excitation of N_2 into short-lived states which cascade into the metastable $N_2(A^3\Sigma_u^+)$ state
2. ionisation of N_2 and O_2
3. dissociation of O_2

The reactions of these species are listed in Appendix A1.2. A large uncertainty in the modelling arises from the poorly known reaction rates. Piper et al. (1981a,b) and others have measured the total rates of quenching of excited N_2. The branching into different products must therefore be estimated. We follow Swider (1976). We also disregard processes such as energy pooling among excited states. These may be important to understand the optical emissions from sprites when comparing with simulations (see Pasko, 2007) but it can be assumed that they do not affect chemistry significantly.

3 Scenarios

To model an event with SIC, both the background conditions (initial conditions) and the rates of excitation, ionisation and dissociation during the event must be known. The selection of typical locations and the derivation of appropriate rates from observations are discussed in the following sections.

3.1 Initial conditions

Runs of the fully time-dependent SIC model require profiles of the initial concentrations of all modelled components. These are obtained by running the model with initial profiles from a run for similar conditions, repeating one 24-h cycle until a quasi-steady state is obtained. For this study the SIC model was initialised for the following conditions:

- Date: August 1–2 (typical northern-hemispheric summer)
- Latitudes: 0°, 40° N, 60° N
- Longitude: 0° (in order for local time to be equal to UT)
- Background ionisation sources: Solar photons, including EUV and soft X-rays, and galactic cosmic rays.
- Low solar and geomagnetic activity, $F_{10.7}=90$, $A_p=10$, for the MSISE-90 neutral background atmosphere. These parameters affect concentrations above 85 km and are therefore of little importance to these scenarios.

Although of minor importance here, three different sets of parameters were also used for the Chabrillat et al. (2002) transport code. The altitude of maximum eddy diffusion was fixed to 110 km, and the following values were selected for the eddy diffusion coefficient and upper boundary density of NO at 150 km:

Equator:. 2.5×10^6 cm^2/s, 1.0×10^7 cm^{-3}

40° N:. 1.2×10^6 cm^2/s, 1.0×10^7 cm^{-3}

60° N:. 1.2×10^6 cm^2/s, 1.0×10^8 cm^{-3}

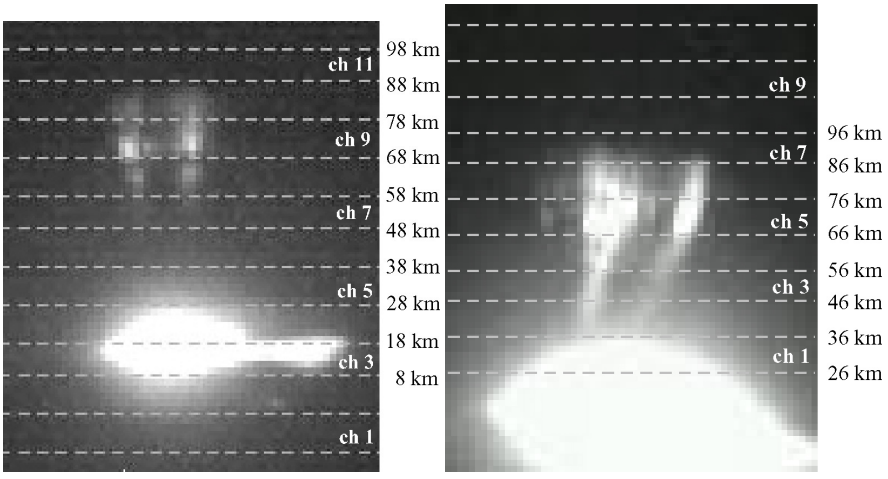

Fig. 2. The sprite events forming the basis of the sprite scenario, as seen by the ISUAL imager. The fields of view of the array photometer channels are outlined. Left figure: The typical case (2004-09-13). Four altitude channels (7–10) provide analysable data. Right figure: The maximal case (2005-07-12). Only altitude channels 5–6 are useful due to contamination from the parent lightning. From Adachi et al. (2006)

3.2 Rates of excitation, ionisation and dissociation

As mentioned, the main difference between the SIC 7 model and previous versions is the capability to include externally calculated rates of the processes listed in Sect. 2.1. For this study we calculate these rates based on data from the Imager of Sprites and Upper-Atmospheric Lightnings (ISUAL) Array Photometer (AP) on FORMOSAT-2 (Chern et al., 2003). Since the AP has a large field of view and therefore measures spatially averaged radiances, an indirect approach is used to calculate the rates. Adachi et al. (2006), henceforth A2006, determined the reduced electric fields (E/n, where n is the air number density) in sprites from red-to-blue spectroscopic ratios. Figure 2 shows two A2006 events, from 2004-09-13 (a typical sprite case) and 2005-07-12 (a maximal sprite case) as seen by the ISUAL imager. Approximate altitudes are marked. Figure 3 reproduces the reduced electric fields calculated in a time resolution of 50 µs.

The retrieved reduced electric fields are subsequently applied to the Bolsig solver (Pitchford et al., 1981), which is based on the two-term Legendre expansion solution of the Boltzmann equation for electrons drifting in a constant electric field. In the Bolsig solver the electrons are assumed to impact upon static nitrogen and oxygen molecules, with cross sections of excitation, ionisation and dissociation given by the Siglo database (CPAT and Kinema Software).

Figures 4 and 5 show the rates obtained from the Bolsig solver. Since the calculated 50-µs series of rates fluctuate rapidly, they have here been smoothed with a 5-point Gaussian window in order to avoid introducing numerical instabilities in the SIC model.

4 Model results

The rates of excitation, ionisation and dissociation retrieved as described above were imposed as single bursts at 00:30 UT on the background atmospheres for the three different latitudes. On average, lightning activity shows a peak between 13 and 20 local hour with a maximum towards the end of the period, i.e. in the evening (Price, 2006). Mesoscale convective systems (MCSs) and complex systems (MCCs) are the strongest sprite producers and are typically observed during the night at mid-latitudes. Imposing the sprite burst during darkness (night-time) is therefore reasonable. In the absence of photochemistry during night-time the chemical balance of the NO_x family is shifted to NO_2, which is observable by emission spectrometers such as the Michelson Interferometer for Passive Atmospheric Sounding (MIPAS) on Envisat (Fischer et al., 2007). An experimental companion study (Arnone et al., 2008b[1]) shows that such enhancements are statistically detectable (see Sect. 5 below). The runs were continued until noon (2 August, 12:00). Figure 6 shows the result for the hour after midnight in the typical case (data from A2006 2004-09-13). Figure 7 shows the full 12-h run for the rates of the maximal A2006 2005-07-12 case. The solid curves show the results of the sprite scenario. The persistence of NO_x in the absence of transport is evident. Control runs without sprite bursts are shown by dashed lines, for comparison. All results are shown for the centre altitudes of the ISUAL array photometer channels

[1] Arnone, E., Kero, A., Dinelli, B. M., Enell, C.-F., Arnold, N. F., Papandrea, E., Rodger, C. J., Carlotti, M., Ridolfi, M., and Turunen, E.: Seeking sprite-induced signatures in remotely sensed middle atmosphere NO_2, Geophys. Res. Lett., in review, 2008b.

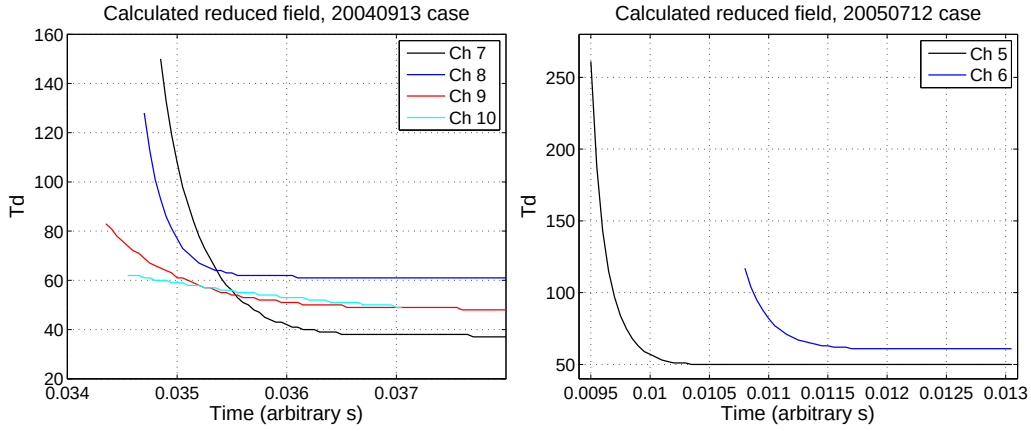

Fig. 3. Reduced electric fields (ratio of E to number density in Townsend units: 1 Td=10^{-17} Vcm^2) calculated from the ISUAL spectroscopic ratios. Left figure: The typical 2004-09-13 case. Right figure: The 2005-07-12 maximal case. Reproduced from Adachi et al. (2006).

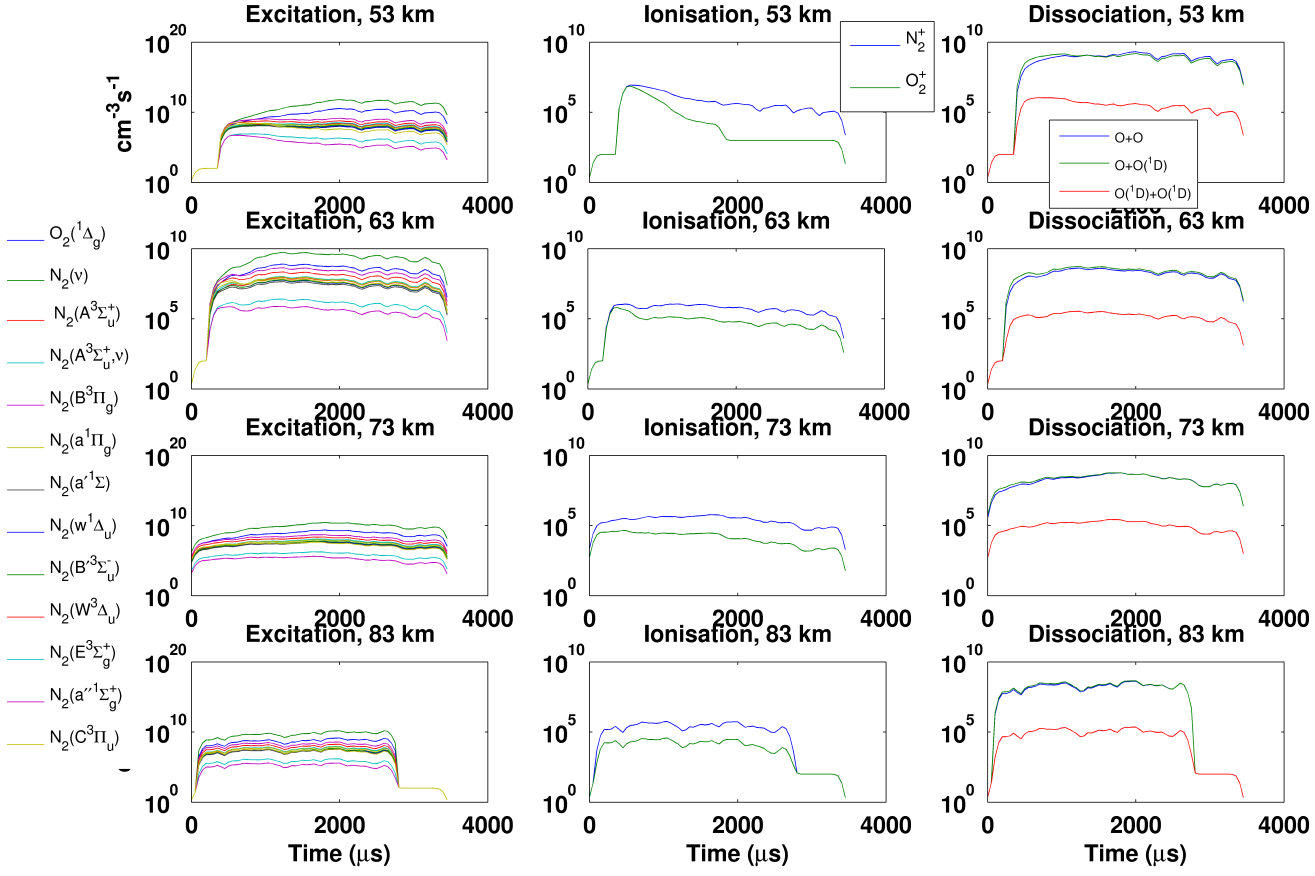

Fig. 4. The rates calculated by the Bolsig Boltzmann solver for the 4 applicable ISUAL altitude channels of the 2004-09-13 case, in 50-μs time resolution. Left columns: rates of excitation of neutral species. Middle column: rates of O_2^+ and N_2^+ ionisation. Right column: Rates of O_2 dissociation. All rates were smoothed with a 5-point Gaussian window.

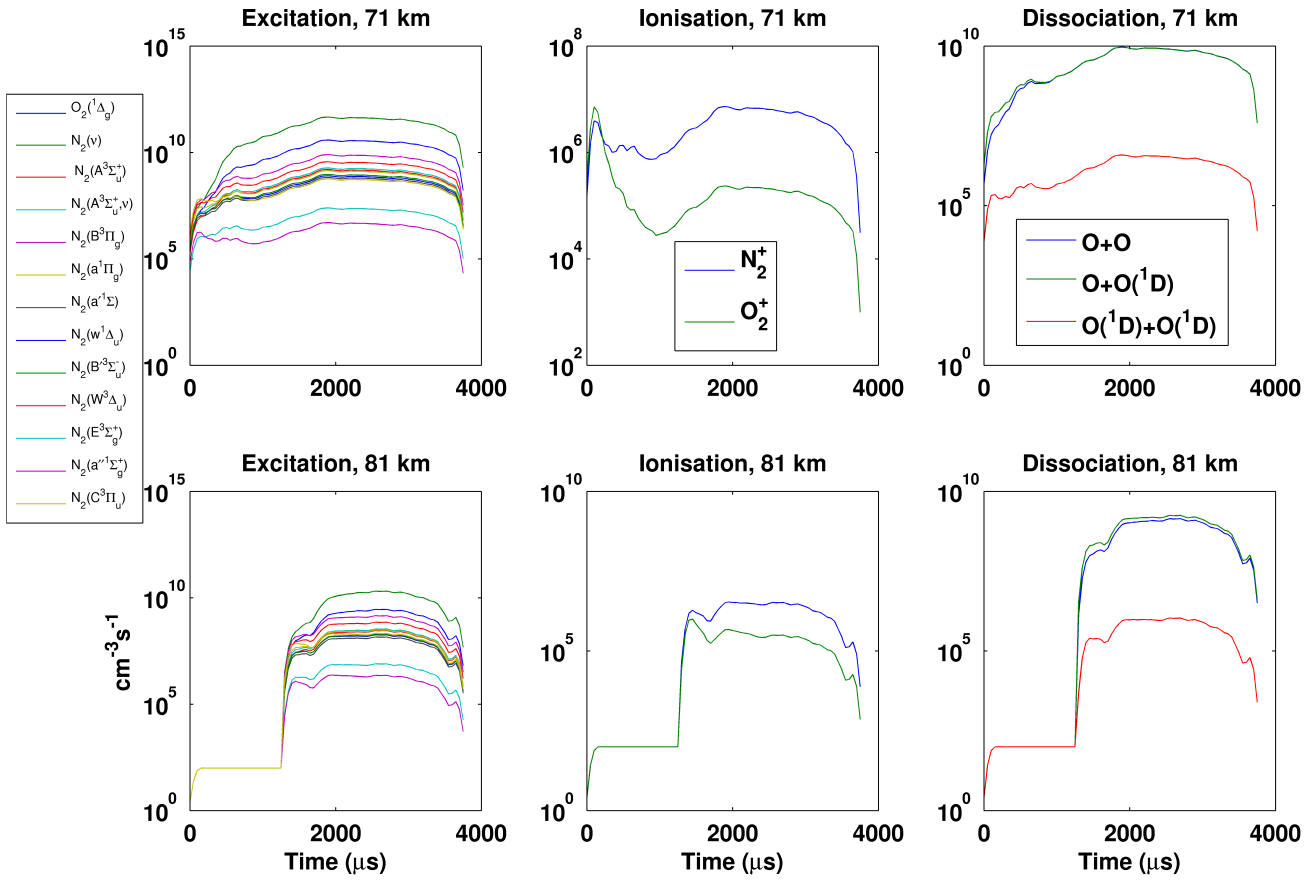

Fig. 5. The rates calculated by the Bolsig Boltzmann solver for the 2 applicable ISUAL altitude channels of the 2005-07-12 case, in 50-μs time resolution. Left columns: rates of excitation of neutral species. Middle column: rates of O_2^+ and N_2^+ ionisation. Right column: Rates of O_2 dissociation. All rates were smoothed with a 5-point Gaussian window.

(Fig. 2). The left columns of the figures show absolute values of NO_x=N+NO+NO_2 and the right columns show the relative enhancements, i.e.

$$\frac{[NO_x] - [NO_x]_{control}}{[NO_x]_{control}} \quad (3)$$

The enhancements of NO_x compared with the control runs, at altitudes around 70 km where the background density is lowest, is at most 50% in the typical case and up to 5–6 times in the maximum case.

Figures 8 and 9 show ozone concentrations for the same scenarios. The runs were continued until the following day (shown here for the maximum case). The effect on ozone, if any, would occur by photochemical reactions starting at sunrise. The figures show a tendency that the increased density of atomic oxygen causes a small buildup of ozone until sunrise, followed by a decrease. However, this case is unrealistic since the dilution of the streamer volumes over the entire sprite volume is completely disregarded. The effect is still below a few percent. Due to model uncertainties, effects of this magnitude are insignificant.

5 Local and global significance

In this section the question of the global significance of the modelled NO_x enhancements is addressed. The significance will be very much affected by

1. the spatial scale of the sprite events (i.e. the volume of air affected)
2. the number of sprites per thunderstorm (which is different in different storms and regions)
3. the wind at the locations of sprite occurrence (with a large seasonal cycle at many latitudes)

Not less important is the question whether the local enhancement would be observable. Space-borne instruments

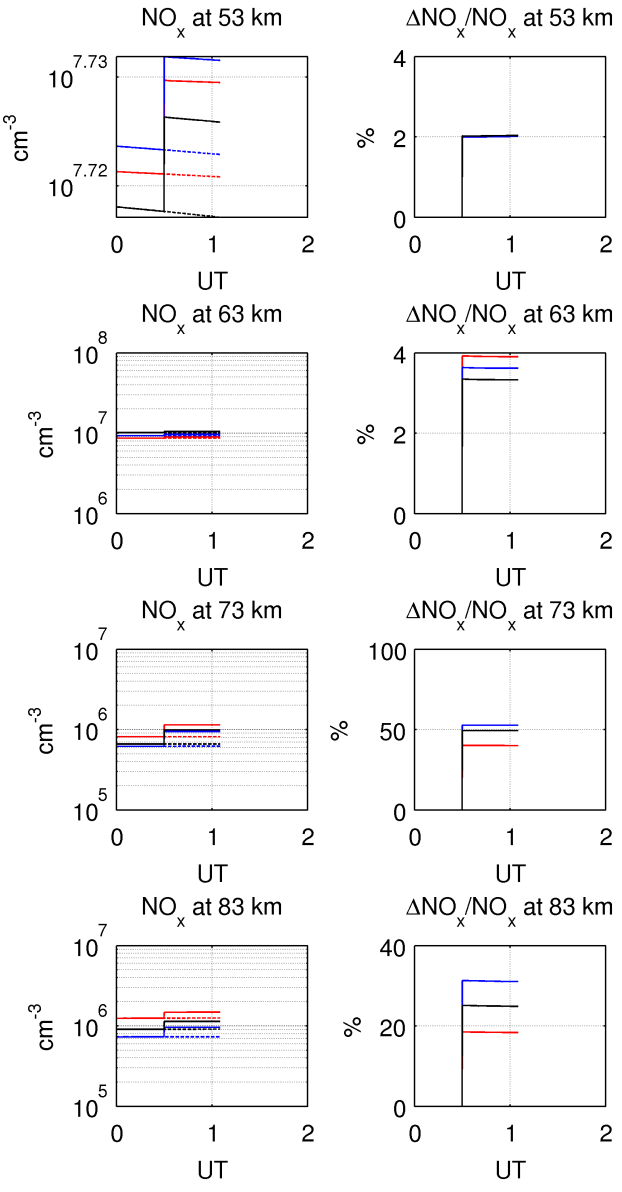

Fig. 6. NO_X for the typical cases (rates based on A2006 2004-09-13 rates) in the 4 available altitude channels. Red: Equator, Blue: 40° N, Black: 60° N. Left column: Absolute concentrations. Right column: Relative changes. Sprite burst starting at 00:30 UT.

provide the only measurements in question for these observations. The aforementioned Envisat/MIPAS experimental study (Arnone et al., 2008b[1]) shows that the statistic local enhancement of NO_2 may be ≈10% at an altitude of 52 km above large thunderstorms.

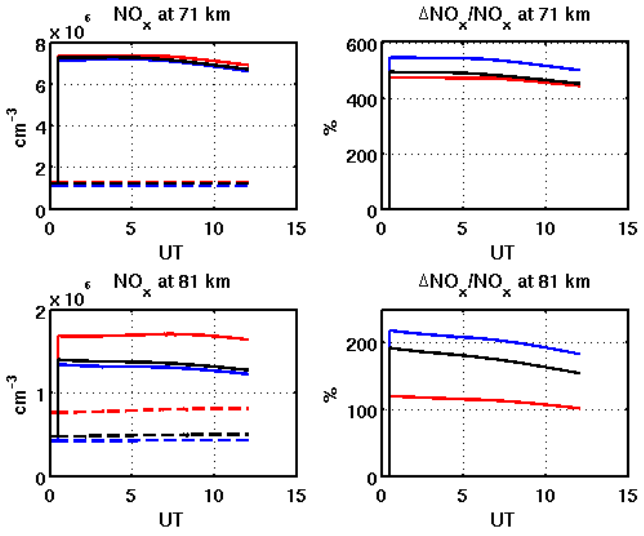

Fig. 7. NO_X for the maximal cases (rates based on A2006 2005-07-12) in the 2 analysable altitude channels. Red: Equator, Blue: 40° N, Black: 60° N. Left column: Absolute concentrations. Right column: Relative changes. Sprite burst starting at 00:30 UT.

5.1 Extrapolation to a sprite event

To state values for parameterisation, which may be of interest in mesoscale modelling, the production of NO_X by a typical sprite must be estimated. The variety of observed sprite morphologies is large, which would require a statistical analysis of the different sprite types and their rate of occurrence, i.e. a large number of global observations that to date are not available. We therefore limit our parameterisation to a first order estimate and assume that the region affected by a sprite is on average $50 \times 50\,km^2$ wide (a sprite area), and extends from 40 to 90 km (leading to a cubic sprite volume). Sprites (or clusters of simultaneous sprites) will be contained within such a volume and the NO_X change within the volume will depend on the fraction of it that is filled with sprite streamers, the filling factor α_f. A representative value $1 \geq \alpha_f \geq 0$ therefore has to be found.

Images of sprites obtained during the recent Eurosprite campaigns (Arnone et al., 2008a) as well as telescopic imaging (Gerken et al., 2000; Gerken and Inan, 2003) can help us to estimate α_f qualitatively. Roughly, measured streamer diameters are in the range 100–200 m, for altitude ranges 60–80 km, where the diffuse region starts. Inspection of carrot sprite images with consideration of these diameters, of the integration of streamer radiance over the exposure time and over the horizontal direction along the line of sight, suggests that the filling factor in the large streamer region (50 km height) is below 10%, possibly ranging between 10^{-3} and 10^{-2}. At the ignition region (70 km height), the bright persistent core (e.g. Cummer et al., 2006) is a much more compact

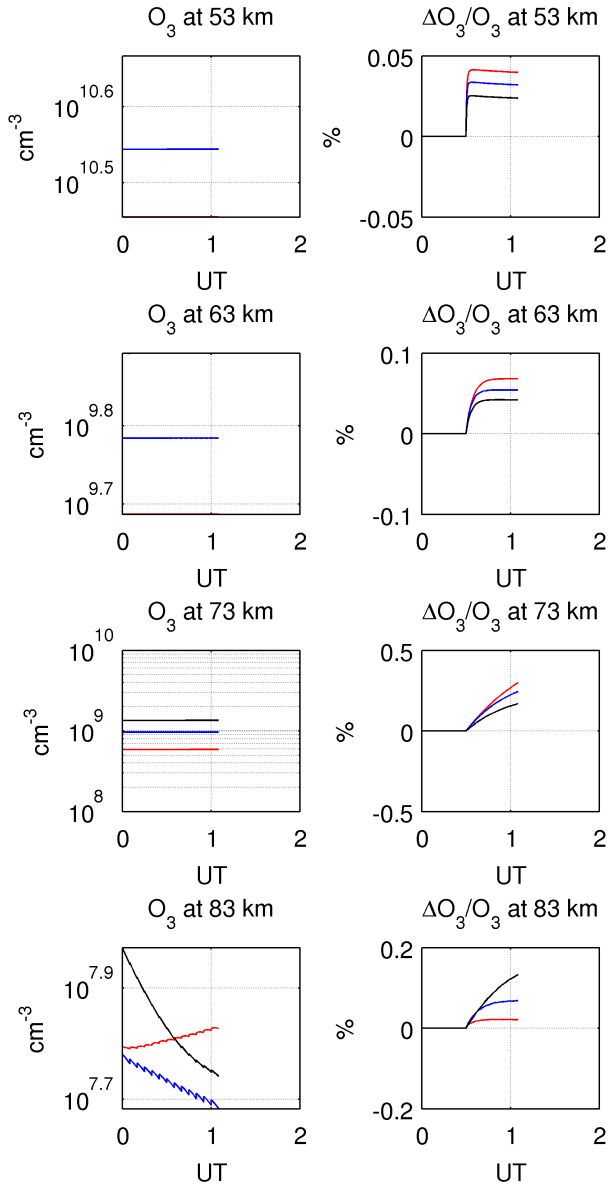

Fig. 8. Ozone for the typical case (A2006 2004-09-13 rates) in the 4 altitude channels. Red: Equator, Blue: 40° N, Black: 60° N. Left column: Absolute concentrations. Right column: Relative changes. Sprite burst starting at 00:30 UT.

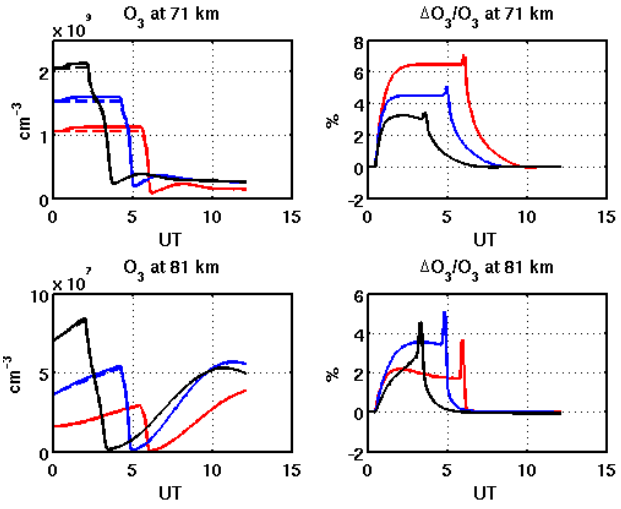

Fig. 9. Ozone for the maximal case (A2006 2005-07-12 rates) in the 2 available altitude channels. Red: Equator, Blue: 40° N, Black: 60° N. Left column: Absolute concentrations. Right column: Relative changes. Sprite burst starting at 00:30 UT.

Table 1. Production of NO_x in a single sprite event, based on the SIC model results of Fig. 6. Filling factors $\alpha_f = 10^{-3}$–10^{-2} and volumes of $50\times50\times10\,km^3$ were assumed.

Altitude range (km)	Typical production (molecules)	Maximal production (molecules)
50–60	5×10^{22}–5×10^{23}	$<5\times10^{24}$
60–70	3×10^{23}–3×10^{24}	$<3\times10^{25}$
70–80	3×10^{22}–3×10^{23}	1.5×10^{23}–1.5×10^{24}
80–90	3×10^{22}–3×10^{23}	3×10^{22}–3×10^{23}

object close to a fully ionised channel (thus similar to columnar sprites): accounting for a 1 km^2 column (or a few of those in case of cluster of sprites), the filling by streamers is constrained to a narrow region of the adopted sprite area, thus filling may be reasonably assumed to be 5×10^{-5}–5×10^{-3}, i.e. 1–10 km^2 over the 50×50 km^2 sprite area.

The estimate in the diffuse uppermost region of a sprite might need a different approach, the filling factor becoming the ratio of the ionisation induced by the sprite glow to that within a modelled streamer. Therefore we will hold the filling as unknown, and use qualitative upper estimates α_f=10^{-3}–10^{-2}.

Using the results of Fig. 6 and the above filling factors, the NO_x production by the type events can be estimated according to Table 1.

Assuming that the productions scale linearly over the lower altitudes and that processes not accounted for in the present SIC modelling, such as hot oxygen atoms and dissociation of molecular nitrogen, can contribute with production rates at most of the same order of magnitude as those obtained here, the NO_x production by a single sprite can be parameterised as 1–10 mol. Ignaccolo et al. (2006) estimated the global rate of sprites to around three per minute. The global production of NO_x by sprites could therefore be taken approximately as 5–50 kmol/day or 150–1500 kg/day. The yearly production is thus up to 10^{31} molecules. As shown below in Table 2, this source is comparable to the strato-

spheric solar proton event production during solar minimum, but much smaller than the global production by cosmic rays or proton events at solar maximum.

As for blue jets, Mishin (1997) has stated an ozone depletion on the order of a percent per event. The number of events observed to date is low. As mentioned, it is an open question whether this is due to the rareness of blue jets or the difficulties of observing blue emissions in the lower atmosphere in presence of clouds. Blue jets can have a significant impact only if they occur frequently. In connection with blue jet events, strong mixing between the troposphere and the stratosphere in the MCSs is also likely to occur.

5.2 Transport of NO_x

The effect of sprite events depends on the dilution by transport of the affected air volume and on the rate of sprite occurrences (i.e. the sprite NO_x source). At the heights considered, meridional and vertical transport, as well as transport by eddy diffusion have timescales of days to months (see e.g. Brasseur and Solomon, 2005). Zonal transport timescales can be as short as a few hours depending on latitude and season, and thus dominate. Typical zonal winds of a few tens of m/s (see e.g. Randel et al., 2004) corresponds to a few thousand kilometres of transport during one night. Considering the distribution of sprite occurrences to resemble that of lightning activity, sprite NO_x sources will be spread over the continents mostly in the tropics. Clearly, depending on zonal winds, one may have either a situation of accumulation of sprite NO_x over individual convective mesoscale systems or one close to zonally averaged. Let us briefly comment on these two extreme situations.

In the first case of buildup above a MCS, one may assume transport to be very inefficient, as the wind speed is only few m/s at the zero wind line close to the equator around solstice or at the tropical edges around equinox. The highest numbers of sprites have been observed above MCSs over the U.S. High Plains (e.g. Lyons, 2006), with peaks of 750 sprites during a 5-hour storm. If sprite NO_x perturbations are persistent over one night, the minimal displacement due to transport over the same period will be of the order of 200 km. Thus, assuming a sprite region of at a minimum 200×50 km and the above sprite area and filling factors, the 750 sprites can almost fill the volume above the MCS completely. This implies that the local NO_x enhancements above the adopted thunderstorm region could reach 50%–500% at the altitude of minimum background density close to 70 km. Clearly, NO_x changes of this magnitude are observable even after mixing with the surrounding air. Even in this case, ozone changes would be small. Furthermore, the required combination of large active MCSs and almost zero wind will occur for a few days per year, given a transition time of a few weeks around equinox or solstice and at most a few large thunderstorms per week.

In the second, more common case of zonally averaged sprite NO_x, one may assume that all sprites occur over the tropics, i.e. a surface of about 250×10^6 km^2, which is a factor 10^5 larger than the adopted sprite area ($50\,\text{km}\times50\,\text{km}$). Accounting for a night of sprite activity at the average rate of three sprites per minute (or 1800 per 10 h) estimated by Ignaccolo et al. (2006), the NO_x enhancement due to sprites can then be considered to be at a maximum on the order of 0.01%, i.e. clearly insignificant.

The results agree qualitatively with the laboratory study presented by Peterson et al. (2005), who concluded that sprites produce less NO_x per event than lightnings. Compared with lightning discharges, the time scale of sprite streamer propagation is short and there is to current understanding little possibility of producing energetic oxygen atoms. However, as was early suggested by Oparin (1952), discharge processes taking place in the reducing atmosphere of early Earth may account for the production of the basic substances of life, such as amino acids. This was confirmed in the now famous experiments of Miller (1953) and by others as well. Since then, the speculation on the role of such processes has continued. It seems that the short-lived nature of TLEs would make them less important than lightning also in this kind of processes, because of the long timescales of the reactions involved, unless there be significant heating by continuing currents also in sprites and jets. We may therefore assume that although the global effects of TLE discharges are likely to be negligible on present-day Earth, these may possibly be more important under other atmospheric conditions found on early Earth or other planets.

5.3 Other variable NO_x sources

Oxidation of nitrous oxide (N_2O) is the major global source of middle-atmospheric NO_x, but occurs mainly below 50 km since N_2O is transported from the troposphere, where it has both natural and artificial sources. Solar-terrestrial coupling, on the other hand, gives rise to long-lived middle and upper atmospheric NO_x sources other than photochemistry, which are significant globally especially at high latitudes. Many studies of satellite data (e.g. Verronen et al., 2002, 2005; Seppälä et al., 2007) have confirmed that solar proton events are an important source of NO_x both in the mesosphere and in the stratosphere, as pointed out for example by Crutzen et al. (1975). In the polar regions, the aurora is also a significant NO_x source which is more or less continuous but highly variable. NO_x from auroras and SPEs is long-lived in the winter polar vortex where it subsides to lower altitudes and subsequently dissolves to lower latitudes as well. This has been confirmed e.g. by Clilverd et al. (2006) and Seppälä et al. (2007). Table 2 gives a summary of the SPE and cosmic ray sources. Transport from the thermosphere is a source of similar magnitude especially in the Southern polar vortex (Vitt et al., 2000a). Comparing with the magnitude of these sources, which all affect sprite altitudes, is clear that global

Table 2. Model estimates of stratospheric and mesospheric total odd nitrogen sources, based on the model study by Vitt and Jackman (1996). The values are total NO_y, which includes also terminal reservoir species such as nitric acid, N_2O_5, and chlorine and bromine nitrate. For this comparison we assume that NO_y=NO_x in the middle atmosphere. Transport from the thermosphere, where odd nitrogen is produced by photochemistry and auroral electrons, is significant mainly at high latitudes. In the stable Antarctic polar vortex the descent of thermospheric odd nitrogen into the stratosphere is comparable with the GCR source, or a few percent of the total high-latitude budget. (Vitt et al., 2000b; Vitt et al., 2000a).

Source	Stratosphere		Mesosphere	
(molec/year)	Min	Max	Min	Max
Solar proton events	8.5×10^{30}	3.3×10^{33}	4.5×10^{30}	5.1×10^{33}
Galactic cosmic rays	3.0×10^{33}	3.7×10^{33}	–	–
N_2O	3.1×10^{34}	3.5×10^{34}	–	–
Current sprite model				1×10^{31}

averaging of the sprite source is nonsensical unless the actual occurrence rate would turn out to be much (1–2 orders of magnitude) larger than the current estimates.

6 Conclusions

Comparing the present model results, as well as observational and laboratory evidence, with the estimated major NO_x sources suggests that sprites are of little global chemical significance. Locally, over large MCSs during limited periods of time, tens of kilogrammes of NO_x could be produced in small volumes ($\approx$100 km scale size). The Envisat/MIPAS observations (Arnone et al., 2008b[1]) also support this conclusion, as small enhancements (some 10%) of NO_2 were detected at 52 km over large thunderstorms. This source can be significant only locally during the periods of low wind speed around equatorial equinox or mid-latitude solstice, when buildup of NO_x in a limited volume of air would be possible. Other transient sources of NO_x are the aurora and solar proton events at high latitudes and intrusions of N_2O from the troposphere at low latitudes. Although variable, these sources are persistent and therefore much more significant than sprites.

Blue jets are much more long-lived than sprites and the possibility that the aforementioned NO_x enhancements observed by airborne measurements above thunderstorms (Baehr et al., 2003) were produced in situ by blue jets is certainly intriguing. Mishin (1997) concluded that a single blue jet may destroy a few percent of the ozone locally. According to available observations, the jets are more rare than sprites and would therefore neither be of any large global importance.

Finally we once again point out that the uncertainties of the present model, arising from omitted processes and unknown reaction rates, are potentially very large, a fact that does not change the conclusions on the global significance of sprites since not even NO_x density enhancements some orders of magnitude higher than those presented here would make the sprite source globally significant. Local enhancements of such magnitudes (implying tenfold or higher NO_x increases) would also very likely have been easily detected, whereas in practice many satellite measurements are required to obtain statistically significant signatures of possible sprite NO_x production, as we demonstrate in Arnone et al. (2008b)[1].

Appendix A

Modifications in SIC 7.3

This appendix summarises the additions specific to the SIC model version 7.3, not described in the previous publications applying SIC version 6 and earlier, listed in the thesis by Verronen (2006).

A1 Excited species

The following excited species can be given as input to SIC 7:
$N_2(\nu)$, $N_2(A^3\Sigma_u^+)$, $N_2(A^3\Sigma_u^+, \nu)$, $N_2(B^3\Pi_g)$, $N_2(a^1\Pi_g)$, $N_2(a'^1\Sigma)$, $N_2(w^1\Delta_u)$, $N_2(B'^3\Sigma_u^-)$, $N_2(W^3\Delta_u)$, $N_2(E^3\Sigma_g^+)$, $N_2(a''^1\Sigma_g^+)$, and $N_2(C^3\Pi_u)$

The main purpose is to allow cascading to the metastable $N_2(A^3\Sigma_u^+)$ state to be treated as pseudo-reactions of these components. $N_2(\nu)$ and $N_2(A^3\Sigma_u^+, \nu)$ represent a crude parameterisation of the dependence of reaction rates on the vibrational state, allowing these components to react faster than the non-vibrationally-excited states.

$O_2(a^1\Delta_g)$ is already included in SIC 6.

A1.1 Cascading

Most of the excited molecular nitrogen states will cascade rapidly to the metastable $N_2(A^3\Sigma_u^+)$ state. To ensure this to work we include the de-excitation channels as reactions (Table A1) with arbitrary but sufficiently high rate coefficients. We disregard the very large dependence on vibrational levels and instead use the Einstein coefficients of the most likely transitions to provide an upper estimate of $N_2(A^3\Sigma_u^+)$ production. The Einstein coefficients of transitions in N_2 are listed in Gilmore et al. (1992).

Table A1. Deexcitation of excited states. N.B.: These rates are estimated from the Einstein coefficients of the fastest vibrational transitions, to provide a maximal estimate of the production of the metastable $N_2(A^3\Sigma_u^+)$ state. Source: Gilmore et al. (1992)

Reaction	Upper state		Lower state	Rate coefficient
D1	$N(^2P)$	$\rightarrow$	N_2	0.0062
D2	$N(^2P)$	$\rightarrow$	$N(^2D)$	0.053
D3	$N(^2D)$	$\rightarrow$	N	$1.9e^{-}05$
D4	$O^+(^2P)$	$\rightarrow$	O^+	0.0522
D5	$O^+(^2P)$	$\rightarrow$	$O^+(^2D)$	0.0907
D6	$O^+(^2D)$	$\rightarrow$	O^+	0.000159
D7	$O(^1S)$	$\rightarrow$	$O(^1D)$	1.26
D8	$O(^1S)$	$\rightarrow$	O	0.0754
D9	$O(^1D)$	$\rightarrow$	O	0.00182
D10	$N^+(^1S)$	$\rightarrow$	$N^+(^1D)$	1.17
D11	$N^+(^1S)$	$\rightarrow$	N^+	0.0315
D12	$N^+(^1D)$	$\rightarrow$	N^+	0.00272
D13	$N_2(A^3\Sigma_u^+)$	$\rightarrow$	N_2	0.5
D14	$N_2(A^3\Sigma_u^+, \nu)$	$\rightarrow$	$N_2(\nu)$	0.52
D15	$O_2(a^1\Delta_g)$	$\rightarrow$	O_2	0.000258
D16	$N_2(B^3\Pi_g)$	$\rightarrow$	$N_2(A^3\Sigma_u^+, \nu)$	50000
D17	$N_2(C^3\Pi_u)$	$\rightarrow$	$N_2(B^3\Pi_g)$	5000000
D18	$N_2(E^3\Sigma_g^+)$	$\rightarrow$	$N_2(A^3\Sigma_u^+, \nu)$	500
D19	$N_2(B'^3\Sigma_u^-)$	$\rightarrow$	$N_2(B^3\Pi_g)$	50000
D20	$N_2(a^1\Pi_g)$	$\rightarrow$	N_2	5000
D21	$O_2^+(A^2\Pi_u)$	$\rightarrow$	O_2^+	200000
D22	$O_2^+(b^4\Sigma_g)$	$\rightarrow$	$O_2^+(a^4\Pi_u)$	200000
D23	$NO(A^2\Sigma)$	$\rightarrow$	NO	100000
D24	$NO(B^2\Pi)$	$\rightarrow$	NO	100000
D25	$NO(C^2\Sigma)$	$\rightarrow$	NO	100000
D26	$N_2^+(A^2\Pi_u)$	$\rightarrow$	N_2^+	50000
D27	$N_2^+(B^2\Sigma_u^+)$	$\rightarrow$	N_2^+	5000000
D28	$N_2(W^3\Delta_u)$	$\rightarrow$	$N_2(B^3\Pi_g)$	200

A1.2 Reactions of excited states

The following tables (Tables A2, A3 and A4) list the reactions of excited states in SIC 7.3 with rate coefficients. The coefficients of reactions not already included in SIC 6 are rough estimates based on available measurements (Piper et al., 1981a,b; Slanger and Black, 1981; Thomas and Kaufman, 1985; Thomas et al., 1987; Pavlov and Buonsanto, 1996). These studies list only total quenching rates of N_2, so the branching into different products must be estimated. The branching ratios are taken from Swider (1976), although this is not much more than an educated guess.

A1.3 Positive ion reactions

Table A2 lists the reactions of excited positive ions included in SIC 7.

A1.4 Neutral-neutral reactions

Table A3 lists reactions of the new excited neutral components included in SIC 7.

A1.5 Recombination

Table A4 lists rates of recombination of the new positive ions included in SIC 7.

A2 Externally calculated rates

The model includes routines to read and include rates of excitation, ionisation and dissociation of N_2 and O_2 calculated by the external Bolsig model (Pitchford et al., 1981) driven by electric fields calculated from ISUAL data.

A2.1 Branching of oxygen dissociation

There are three possible branches of O_2 dissociation:

$$O_2 \rightarrow 2O \quad \text{(R3)}$$

$$O_2 \rightarrow O + O(^1D) \quad \text{(R4)}$$

$$O_2 \rightarrow 2O(^1D) \quad \text{(R5)}$$

Table A2. Reactions of excited positive ions included in SIC 7.

Reaction	Reactants		Products	Rate coefficient
P1	$O_2^+(a^4\Pi_u) + N_2$	$\rightarrow$	$N_2^+ + O_2$	2.0×10^{-10}
P2	$O_2^+(a^4\Pi_u) + O$	$\rightarrow$	$O_2^+ + O$	1.0×10^{-10}
P3	$O_2^+(b^4\Sigma_g) + N_2$	$\rightarrow$	$N_2^+ + O_2$	2.0×10^{-10}
P4	$O_2^+(b^4\Sigma_g) + O$	$\rightarrow$	$O_2^+ + O$	1.0×10^{-10}
P5	$O_2^+(A^2\Pi_u) + N_2$	$\rightarrow$	$N_2^+ + O_2$	2.0×10^{-10}
P6	$O_2^+(A^2\Pi_u) + O$	$\rightarrow$	$O_2^+ + O$	1.0×10^{-10}
P7	$N_2^+(A^2\Pi_u) + O$	$\rightarrow$	$NO^+ + N(^2D)$	$1.4\times10^{-10}\times(300/T)^{0.44}$
P8	$N_2^+(A^2\Pi_u) + O$	$\rightarrow$	$O^+ + N_2$	$9.8\times10^{-12}\times(300/T)^{0.23}$
P9	$N_2^+(A^2\Pi_u) + O_2$	$\rightarrow$	$O_2^+ + N_2$	$5\times10^{-11}\times(300/T)^{0.8}$
P10	$N_2^+(A^2\Pi_u) + NO$	$\rightarrow$	$NO^+ + N_2$	3.3×10^{-10}

Table A3. Reactions of the new excited neutral components included in SIC 7. The $N(^2D)$, $O(^1D)$ and $O_2(^1\Delta_g)$ states are included in SIC 6.

Reaction	Reactants		Products	Rate coefficient
N1	$N_2(v) + O_2$	$\rightarrow$	$N_2 + O_2$	10^{-16}
N2	$N_2(A^3\Sigma_u^+) + O_2$	$\rightarrow$	$N_2 + O_2$	$0.2\times2.5\times10^{-12}$
N3	$N_2(A^3\Sigma_u^+) + O_2$	$\rightarrow$	$N_2 + O + O$	$0.2\times2.5\times10^{-12}$
N4	$N_2(A^3\Sigma_u^+) + O_2$	$\rightarrow$	$N_2O + O$	$0.4\times2.5\times10^{-12}$
N5	$N_2(A^3\Sigma_u^+) + O_2$	$\rightarrow$	$N_2O + O(^1D)$	$0.2\times2.5\times10^{-12}$
N6	$N_2(A^3\Sigma_u^+,v) + O_2$	$\rightarrow$	$N_2(A_3\Sigma_u^+) + O_2$	10^{-16}
N7	$N_2(A^3\Sigma_u^+,v) + O_2$	$\rightarrow$	$N_2 + O_2$	$0.2\times4.5\times10^{-12}$
N8	$N_2(A^3\Sigma_u^+,v) + O_2$	$\rightarrow$	$N_2 + O + O$	$0.2\times4.5\times10^{-12}$
N9	$N_2(A^3\Sigma_u^+,v) + O_2$	$\rightarrow$	$N_2O + O$	$0.4\times4.5\times10^{-12}$
N10	$N_2(A^3\Sigma_u^+,v) + O_2$	$\rightarrow$	$N_2O + O(^1D)$	$0.2\times4.5\times10^{-12}$
N11	$N_2(v) + O$	$\rightarrow$	$N_2 + O$	$1.07\times10^{-10}\times e^{-69.9/T^{1/3}}$
N12	$N_2(A^3\Sigma_u^+) + O$	$\rightarrow$	$N_2 + O$	$0.05\times2.8\times10^{-11}$
N13	$N_2(A^3\Sigma_u^+) + O$	$\rightarrow$	$N_2 + O(^1D)$	$0.05\times2.8\times10^{-11}$
N14	$N_2(A^3\Sigma_u^+) + O$	$\rightarrow$	$N_2 + O(^1S)$	$0.2\times2.8\times10^{-11}$
N15	$N_2(A^3\Sigma_u^+) + O$	$\rightarrow$	$NO + N$	$0.3\times2.8\times10^{-11}$
N16	$N_2(A^3\Sigma_u^+) + O$	$\rightarrow$	$NO + N(^2D)$	$0.4\times2.8\times10^{-11}$
N17	$N_2(A^3\Sigma_u^+,v) + O$	$\rightarrow$	$N_2 + O$	$0.05\times5.0\times10^{-11}$
N18	$N_2(A^3\Sigma_u^+,v) + O$	$\rightarrow$	$N_2 + O(^1D)$	$0.05\times5.0\times10^{-11}$
N19	$N_2(A^3\Sigma_u^+,v) + O$	$\rightarrow$	$N_2 + O(^1S)$	$0.2\times5.0\times10^{-11}$
N20	$N_2(A^3\Sigma_u^+,v) + O$	$\rightarrow$	$NO + N$	$0.3\times5.0\times10^{-11}$
N21	$N_2(A^3\Sigma_u^+,v) + O$	$\rightarrow$	$NO + N(^2D)$	$0.4\times5.0\times10^{-11}$
N22	$O_2 + O(^1S)$	$\rightarrow$	$O_2 + O$	3×10^{-13}
N23	$O_2(a^1\Delta_g) + O(^1S)$	$\rightarrow$	$O_2 + O$	1.7×10^{-10}
N24	$N_2(a'^1\Sigma) + N_2$	$\rightarrow$	$N_2 + N_2$	1.9×10^{-13}
N25	$N_2(a'^1\Sigma) + O_2$	$\rightarrow$	$N_2 + O_2$	2.8×10^{-11}
N26	$N_2(B^3\Pi_g) + O_2$	$\rightarrow$	$N_2 + O_2$	2×10^{-10}
N27	$N_2(a''^1\Sigma_g^+) + O_2$	$\rightarrow$	$N_2 + O_2$	2.8×10^{-11}
N28	$N_2(w^1\Delta_u) + O_2$	$\rightarrow$	$N_2 + O_2$	2.8×10^{-11}

Table A4. Recombination of new positive ions in SIC 7.

Reaction	Reactants		Products	Rate coefficient
Re1	$O_2^+ + e$	$\rightarrow$	$O + O(^1S)$	$0.1\times2.2\times10^{-7}\times(300/Te)^5$
Re2	$O^+(^2P) + e$	$\rightarrow$	$O^+ + e$	3×10^{-8}
Re3	$O_2^+(a^4\Pi_u) + e$	$\rightarrow$	$O_2^+ + e$	1×10^{-7}

Acknowledgements. C.-F. Enell, E. Arnone and O. Chanrion acknowledge funding through the European Community's Human Potential Programme under contract HPRN-CT-2002-00216, Coupling of Atmospheric Layers, during 2003–2006. C.-F. Enell is presently funded by the Academy of Finland through project 109054, "Solar Energetic Radiation and Chemical Aeronomy of the Mesosphere". P. T. Verronen was partly funded by the Academy of Finland through the ANTARES space research programme.

The work was also supported by a travel grant to E. Arnone from the Vilho, Yrjö and Kalle Väisälä Foundation of the Finnish Academy of Science and Letters.

Topical Editor U.-P. Hoppe thanks M. Sinnhuber and another anonymous referee for their help in evaluating this paper.

References

Adachi, T., Fukunishi, H., Takahashi, Y., Hiraki, Y., Hsu, R.-R., Su, H.-T., Chen, A. B., Mende, S. B., Frey, H. U., and Lee, L. C.: Electric field transition between the diffuse and streamer regions of sprites estimated from ISUAL/array photometer measurements, Geophys. Res. Lett., 33, L17803, doi:10.1029/2006GL026495, 2006.

Arnone, E., Berg, P., Boberg, F., Bór, J., Chanrion, O., Enell, C.-F., Ignaccolo, M., Mika, Á., Odzimek, A., van der Velde, O., Farges, T., Laursen, S., Neubert, T., and Sátori, G.: The Eurosprite 2005 campaign, in: Proceedings of the 33rd Annual European meeting on Atmospheric Studies by Optical Methods (33AM), edited by: Arvelius, J., no. 292 in IRF Scientific Reports, Swedish Inst. of Space Physics, Kiruna, in press, 2008a.

Baehr, J., Schlager, H., Ziereis, H., Stock, P., van Velthoven, P., Busen, R., Ström, J., and Schumann, U.: Aircraft observations of NO, NO_y, CO, and O_3 in the upper troposphere from 60° N to 60° S – Interhemispheric differences, Geophys. Res. Lett., 30, 1598, doi:10.1029/2003GL016935, 2003.

Balakrishnan, N. and Dalgarno, A.: Nitric oxide production in collisions of hot $O(^3P)$ atoms with N_2, J. Geophys. Res., 108, 1065, doi:10.1029/2002JA009566, 2003.

Banks, P. and Kockarts, G.: Aeronomy, Academic Press Inc., 1973.

Birkeland, K.: Norwegian Aurora Polaris Expedition; 1902–3, vol. 1, H. Aschehoug and Co., Christiania, Norway, 1908.

Brasseur, G. P. and Solomon, S.: Aeronomy of the Middle Atmosphere, Springer Verlag, The Netherlands, 2005.

Bucsela, E., Morrill, J., Heavner, M., Siefring, C., Berg, S., Hampton, D., Moudry, D., Wescott, E., and Sentman, D.: $N_2(B^3\Pi_g)$ and $N_2^+(A^2\Pi_u)$ vibrational distributions observed in sprites, J. Atmos. and Solar-Terr. Phys., 65, 583–591, 2003.

Callis, L. B., Natarajan, M., and Lambeth, J. D.: Observed and calculated mesospheric NO, 1992-1997, Geophys. Res. Lett., 29, 1030, doi:10.1029/2001GL013995, 2002.

Chabrillat, S., Kockarts, G., Fonteyn, D., and Brasseur, G.: Impact of molecular diffusion on the CO_2 distribution and the temperature in the mesosphere, Geophys. Res. Lett., 29, 1729, doi:10.1029/2002GL015309, 2002.

Chern, J. L., Hsu, R.-R., Su, H.-T., Mende, S. B., Fukunishi, H., Takahashi, Y., and Lee, L. C.: Global survey of upper atmospheric transient luminous events on the ROCSAT-2 satellite, J. Atmos. Sol.-Terr. Phy., 65, 647–659, 2003.

Clilverd, M. A., Seppälä, A., Rodger, C. J., Verronen, P. T., and Thomson, N. R.: Ionospheric evidence of thermosphere-to-stratosphere descent of polar NO_x, Geophys. Res. Lett., 33, L19811, doi:10.1029/2006GL026727, 2006.

Coppens, F., Berton, R., Bondiou-Clergerie, A., and Gallimberti, I.: Theoretical estimate of NO_x production in lightning corona, J. Geophys. Res., 103, 10 769–10 785, 1998.

CPAT and Kinema Software: The Siglo data base, http://www.siglo-kinema.com.

Crutzen, P. J., Isaksen, I. S. A., and Reid, G. C.: Solar Proton Events: Stratospheric Sources of Nitric Oxide, Science, 189, 457–458, 1975.

Cummer, S. A., Jaugey, N., Li, J., Lyons, W. A., Nelson, T. E., and Gerken, E. A.: Submillisecond imaging of sprite development and structure, Geophys. Res. Lett., 33, L04104, doi:10.1029/2005GL024969, 2006.

Fischer, H., Birk, M., Blom, C., Carli, B., Carlotti, M., von Clarmann, T., Delbouille, L., Dudhia, A., Ehhalt, D., Endemann, M., Flaud, J. M., Gessner, R., Kleinert, A., Koopmann, R., Langen, J., López-Puertas, M., Mosner, P., Nett, H., Oelhaf, H., Perron, G., Remedios, J., Ridolfi, M., Stiller, G., and Zander, R.: MIPAS: an instrument for atmospheric and climate research, Atmos. Chem. Phys. Discuss., 7, 8795–8893, 2007.

Franz, R. C., Nemzek, R. J., and Winckler, J. R.: Television Image of a Large Upward Electrical Discharge Above a Thunderstorm System, Science, 249, 48–51, 1990.

Fukunishi, H., Takahashi, Y., Kubota, M., and Sakanoi, K.: Elves: Lightning induced transient luminous events in the lower ionosphere,, Geophys. Res. Lett., 23, 2157–2160, doi:10.1029/96GL01979, 1996.

Funke, B., López-Puertas, M., von Clarmann, T., Stiller, G. P., Fischer, H., Glatthor, N., Grabowski, U., Höpfner, M., Kellmann, S., Kiefer, M., Linden, A., Mengistu Tsidu, G., Milz, M., Steck, T., and Wang, D. Y.: Retrieval of stratospheric NO_x from 5.3 and 6.2 μm nonlocal thermodynamic equilibrium emissions measured by Michelson Interferometer for Passive Atmospheric Sounding (MIPAS) on Envisat, J. Geophys. Res., 110, D09302, doi:10.1029/2004JD005225, 2005.

Gerken, E. A. and Inan, U. S.: Observations of decameter-scale morphologies in sprites, J. Atmos. Sol.-Terr. Phy., 65, 567–572, 2003.

Gerken, E. A., Inan, U. S., and Barrington-Leigh, C. P.: Telescopic imaging of sprites, Geophys. Res. Lett., 27, 2637–2640, 2000.

Gilmore, F. R., Laher, R. R., and Espy, P. J.: Franck-Condon Factors, r-Centroids, Electronic transition Moments, and Einstein Coefficients for many Nitrogen and oxygen Band Systems, J. Phys. Chem. Ref. Data, 21, 1005–1107, 1992.

Hedin, A. E.: Extension of the MSIS Thermospheric Model into the Middle and Lower Atmosphere, J. Geophys. Res., 96, 1159–1172, 1991.

Hiraki, Y., Tong, L., Fukunishi, H., Nanbu, K., Kasai, Y., and Ichimura, A.: Generation of metastable oxygen atom $O(^1D)$ in sprite halos, Geophys. Res. Lett., 31, L14105, doi:10.1029/2004GL020048, 2004.

Huntrieser, H., Schlager, H., Roiger, A., Lichtenstern, M., Schumann, U., Kurz, C., Brunner, D., Schwierz, C., Richter, A., and Stohl, A.: Lightning-produced NOx over Brazil during TROCCINOX: Airborne measurements in tropical and subtropical thunderstorms and the importance of mesoscale convective systems, Atmos. Chem. Phys., 7, 2987–3013, 2007.

Ignaccolo, M., Farges, T., Mika, A., Allin, T. H., Chanrion, O., Blanc, E., Fraser-Smith, A. C., and Füllekrug, M.: The Planetary Rate of Sprite Events, Geophys. Res. Lett., 33, L11808, doi:10.1029/2005GL025502, 2006.

Liu, N., Pasko, V. P., Burkhardt, D. H., Frey, H. U., Mende, S. B., Su, H.-T., Chen, A. B., Hsu, R.-R., Lee, L.-C., Fukunishi, H., and Takahashi, Y.: Comparison of results from sprite streamer modeling with spectrophotometric measurements by ISUAL instrument on FORMOSAT-2 satellite, Geophys. Res. Lett., 33, L01101, doi:10.1029/2005GL024243, 2006.

Lyons, W. A.: The meteorology of transient luminous events – an introduction and overview, in: Sprites, Elves and Intense Lightning Discharges, edited by: Füllekrug, M., Mareev, E. A., and Rycroft, M. J., vol. 225 of *NATO Science Series II. Mathematics, physics and chemistry*, pp. 19–56, Springer Verlag, ISBN 1-4020-4628-6, 2006.

Mende, S., Rairden, R., Swenson, G., and Lyons, A.: Sprite spectra; N_2 1 PG band identification, Geophys. Res. Lett., 22, 2633–2636, 1995.

Mende, S. B., Frey, H. U., Hsu, R. R., Su, H. T., Chen, A. B., Lee, L. C., Sentman, D. D., Takahashi, Y., and Fukunishi, H.: D region ionization by lightning-induced electromagnetic pulses, J. Geophys. Res., 110, A11312, doi:10.1029/2005JA011064, 2005.

Miller, S. L.: A Production of Amino Acids Under Possible Primitive Earth Conditions, Science, 117, 528–529, 1953.

Mishin, E.: Ozone layer perturbation by a single blue jet, Geophys. Res. Lett., 24, 1919–1922, 1997.

Morrill, J. S., Bucsela, E. J., Pasko, V. P., Berg, S. L., Heavner, M. J., Moudry, D. R., Benesch, W. M., Wescott, E. M., and Sentman, D. D.: Time resolved N_2 triplet state vibrational populations and emissions associated with red sprites, J. Atmos. Sol.-Terr. Phy., 60, 811–829, 1998.

Neubert, T.: On Sprites and Their Exotic Kin, Science, 300, 747–749, 2003.

Noxon, J. F.: Atmospheric nitrogen fixation by lightning, Geophys. Res. Lett., 3, 463–465, 1976.

Oparin, A. I.: The origin of life, Dover, New York, 1952.

Pasko, V. P.: Red sprite discharges in the atmosphere at high altitude: the molecular physics and the similarity with laboratory discharges, Plasma Sources Sci. Technol., 16, S13–S29, doi:10.1088/0963-0252/16/1/S02, 2007.

Pavlov, A. V. and Buonsanto, M. J.: Using steady state vibrational temperatures to model effects of N_2^* on calculations of electron densities, J. Geophys. Res., 101, 26 941–26 946, doi:10.1029/96JA02734, 1996.

Peterson, H., Bailey, M., Hallett, J., and Beasley, W.: NOx Production in Simulated Blue Jets, Sprites, and TLE Discharges, AGU Fall Meeting Abstracts, pp. A990, 2005.

Piper, L. G., Caledonia, G. E., and Kennealy, J. P.: Rate constants for deactivation of $N_2(A,\nu' = 0, 1)$ by O_2, J. Chem. Phys., 74, 2888–2895, 1981a.

Piper, L. G., Caledonia, G. E., and Kennealy, J. P.: Rate constants for deactivation of $N_2(A^3\Sigma_u^+, \nu = 0, 1)$ by O, J. Chem. Phys., 75, 2847–2852, 1981b.

Pitchford, L. C., Oneil, S. V., and J. R. Rumble, J.: Extended Boltzmann analysis of electron swarm experiments, Phys. Rev. A, 23, 294–304, 1981.

Press, W. H., Teukolsky, S. A., Vetterling, W. T., and Flannery, B. P.: Numerical Recipes in C, Cambridge University Press, second edn., 1992.

Price, C.: Global thunderstorm activity, in: Sprites, Elves and Intense Lightning Discharges, edited by: Füllekrug, M., Mareev, E. A., and Rycroft, M. J., vol. 225 of *NATO Science Series II. Mathematics, physics and chemistry*, Springer Verlag, ISBN 1-4020-4628-6, 2006.

Rakov, V. A. and Uman, M. A.: Lightning, Physics and Effects, Cambridge University Press, ISBN: 0-521-58327-6, 2003.

Randel, W., Udelhofen, P., Fleming, E., Geller, M., Gelman, M., Hamilton, K., Karoly, D., Ortland, D., Pawson, S., Swinbank, R., Wu, F., Baldwin, M., Chanin, M.-L., Keckhut, P., Labitzke, K., Remsberg, E., Simmons, A., and Wu, D.: The SPARC Intercomparison of Middle-Atmosphere Climatologies, J. Climate, 17, 986–1003, 2004.

Schumann, U. and Huntrieser, H.: The global lightning-induced nitrogen oxides source, Atmos. Chem. Phys., 7, 3823–3907, 2007.

Sentman, D. D., Wescott, E. M., Osborne, D. L., Hampton, D. L., and Heavner, M. J.: Preliminary results from the Sprites94 aircraft campaign: 1. Red sprites, Geophys. Res. Lett., 22, 1205–1208, 1995.

Seppälä, A., Clilverd, M. A., and Rodger, C. J.: NO_x enhancements in the middle atmosphere: The relative significance of Solar Proton Events and the Aurora as a source, J. Geophys. Res., 112, D23303, doi:10.1029/2006JD008326, 2007.

Shimazaki, T.: Minor Constituents in the Middle Atmosphere, no. 6 in Developments in Earth and Planetary Physics, D. Reidel Publishing Company, 1984.

Slanger, T. G. and Black, G.: Quenching of $O(^1S)$ by $O_2(a^1\Delta_g)$, Geophys. Res. Lett., 8, 535–538, 1981.

Stenbaek-Nielsen, H.-C., McHarg, M. G., Kammae, T., and Sentman, D. D.: Observed Emission Rates in Sprite Streamer Heads, Geophys. Res. Lett., 34(11), L11105, doi:10.1029/2007GL029881, 2007.

Su, H. T., Hsu, R. R., Chen, A. B., Wang, Y. C., Hsiao, W. S., Lai, W. C., Lee, L. C., Sato, M., and Fukunishi, H.: Gigantic jets between a thundercloud and the ionosphere, Nature, 423, 974–976, 2003.

Swider, W.: Atmospheric formation of NO from $N_2(A^3\Sigma)$, Geophys. Res. Lett., 3, 335–337, 1976.

Thomas, J. M. and Kaufman, F.: Rate constants of the reactions of metastable $N_2(A^3\Sigma_u^+)$ in ν=0,1,2, and 3 with ground state O_2 and O, J. Chem. Phys., 83, 2900–2903, 1985.

Thomas, J. M., Kaufman, F., and Golde, M. F.: Rate constants for electronic quenching of $N_2(A^3\Sigma_u^+, \nu = 0 - 6)$ by O_2, NO, CO, N_2O, and C_2H_4, J. Chem. Phys., 86, 6885–6892, 1987.

Tobiska, W., Woods, T., Eparvier, F., Viereck, R., Floyd, L., Bouwer, D., Rottman, G., and White, O.: The SOLAR2000 empirical solar irradiance model and forecast tool, J. Atmos. Sol.-Terr. Phy., 62, 1233–1250, 2000.

Turunen, E., Matveinen, H., Tolvanen, J., and Ranta, H.: D-Region Ion Chemistry Model, in: STEP Handbook of Ionospheric Models, edited by Schunk, R. W., pp. 1–25, Scientific Committee on Solar-Terrestrial Physics, 1996.

Verronen, P., Turunen, E., Ulich, T., and Kyrölä, E.: Modelling the effects of the October 1989 solar proton event on mesospheric odd nitrogen using a detailed ion and neutral chemistry model, Ann. Geophys., 20, 1967–1976, 2002.

Verronen, P. T.: Ionosphere-atmosphere interaction during solar proton events, Ph.D. thesis, Finnish Meteorological Institute, Helsinki, Finland, http://ethesis.helsinki.fi/, ISBN: 951-697-650-6, 2006.

Verronen, P. T., Seppälä, A., Clilverd, M. A., Rodger, C. J., Kyrölä, E., Enell, C.-F., Ulich, T., and Turunen, E.: Diurnal variation of ozone depletion during the October–November 2003 solar proton event, J. Geophys. Res., 110, A09S32, doi:10.1029/2004JA010932, 2005.

Vitt, F. M. and Jackman, C. H.: A comparison of sources of odd nitrogen production from 1974 through 1993 in the Earth's middle atmosphere as calculated using a two-dimensional model, J. Geophys. Res., 101, 6729–6739, 1996.

Vitt, F. M., Armstrong, T. P., Cravens, T. E., Dreschhoff, G. A. M., Jackman, C. H., and Laird, C. M.: Computed contributions to odd nitrogen concentrations in the Earth's polar middle atmosphere by energetic charged particles, J. Atmos. Sol.-Terr. Phy., 62, 669–683, 2000a.

Vitt, F. M., Cravens, T. E., and Jackman, C. H.: A two-dimensional model of thermospheric nitric oxide sources and their contributions to the middle atmospheric chemical balance, J. Atmos. Sol.-Terr. Phy., 62, 653–667, 2000b.